

Formaldehyde
production from
isoprene oxidation
across NO_x regimes

G. M. Wolfe et al.

This discussion paper is/has been under review for the journal Atmospheric Chemistry and Physics (ACP). Please refer to the corresponding final paper in ACP if available.

Formaldehyde production from isoprene oxidation across NO_x regimes

G. M. Wolfe^{1,2}, J. Kaiser³, T. F. Hanisco², F. N. Keutsch⁴, J. A. de Gouw^{5,6}, J. B. Gilman^{5,6}, M. Graus^{5,6,a}, C. D. Hatch⁷, J. Holloway^{5,6}, L. W. Horowitz⁸, B. H. Lee⁹, B. M. Lerner^{5,6}, F. Lopez-Hilfiker⁹, J. Mao^{8,11}, M. R. Marvin¹⁰, J. Peischl^{5,6}, I. B. Pollack^{5,6}, J. M. Roberts⁶, T. B. Ryerson⁶, J. A. Thornton⁹, P. R. Veres^{5,6}, and C. Warneke^{5,6}

¹Joint Center for Earth Systems Technology, University of Maryland Baltimore County, Baltimore, MD, USA

²Atmospheric Chemistry and Dynamics Laboratory, NASA Goddard Space Flight Center, Greenbelt, MD, USA

³Department of Chemistry, University of Wisconsin-Madison, Madison, WI, USA

⁴School of Engineering and Applied Sciences and Department of Chemistry and Chemical Biology, Harvard University, Cambridge, MA, USA

⁵Cooperative Institute for Research in Environmental Sciences, University of Colorado Boulder, Boulder, CO, USA

⁶Chemical Sciences Division, NOAA Earth System Research Laboratory, Boulder, CO, USA

⁷Department of Chemistry, Hendrix College, Conway, AR, USA

⁸NOAA Geophysical Fluid Dynamics Laboratory, Princeton, NJ, USA

Title Page

Abstract

Introduction

Conclusions

References

Tables

Figures



Back

Close

Full Screen / Esc

Printer-friendly Version

Interactive Discussion



⁹Department of Atmospheric Sciences, University of Washington, Seattle, WA, USA

¹⁰Department of Chemistry, University of Maryland, College Park, MD, USA

¹¹Program in Atmospheric and Oceanic Sciences, Princeton University, Princeton, NJ, USA

^anow at: Institute of Atmospheric and Cryospheric Sciences, Innsbruck University, Austria

Received: 28 October 2015 – Accepted: 31 October 2015 – Published: 11 November 2015

Correspondence to: G. M. Wolfe (glenn.m.wolfe@nasa.gov)

Published by Copernicus Publications on behalf of the European Geosciences Union.

**Formaldehyde
production from
isoprene oxidation
across NO_x regimes**

G. M. Wolfe et al.

Title Page

Abstract

Introduction

Conclusions

References

Tables

Figures



Back

Close

Full Screen / Esc

Printer-friendly Version

Interactive Discussion



Abstract

The chemical link between isoprene and formaldehyde (HCHO) is a strong, non-linear function of NO_x ($= \text{NO} + \text{NO}_2$). This relationship is a linchpin for top-down isoprene emission inventory verification from orbital HCHO column observations. It is also a benchmark for overall mechanism performance with regard to VOC oxidation. Using a comprehensive suite of airborne in situ observations over the Southeast US, we quantify HCHO production across the urban-rural spectrum. Analysis of isoprene and its major first-generation oxidation products allows us to define both a “prompt” yield of HCHO (molecules of HCHO produced per molecule of freshly-emitted isoprene) and the background HCHO mixing ratio (from oxidation of longer-lived hydrocarbons). Over the range of observed NO_x values (roughly 0.1–2 ppbv), the prompt yield increases by a factor of 3 (from 0.3 to 0.9 ppbv ppbv⁻¹), while background HCHO increases by more than a factor of 2 (from 1.5 to 3.3 ppbv). We apply the same method to evaluate the performance of both a global chemical transport model (AM3) and a measurement-constrained 0-D chemical box model. Both models reproduce the NO_x dependence of the prompt HCHO yield, illustrating that models with updated isoprene oxidation mechanisms can adequately capture the link between HCHO and recent isoprene emissions. On the other hand, both models under-estimate background HCHO mixing ratios, suggesting missing HCHO precursors, inadequate representation of later-generation isoprene degradation and/or under-estimated hydroxyl radical concentrations. Moreover, we find that the total organic peroxy radical production rate is essentially independent of NO_x , as the increase in oxidizing capacity with NO_x is largely balanced by a decrease in VOC reactivity. Thus, the observed NO_x dependence of HCHO mainly reflects the changing fate of organic peroxy radicals.

Formaldehyde production from isoprene oxidation across NO_x regimes

G. M. Wolfe et al.

Title Page

Abstract

Introduction

Conclusions

References

Tables

Figures



Back

Close

Full Screen / Esc

Printer-friendly Version

Interactive Discussion



Formaldehyde production from isoprene oxidation across NO_x regimes

G. M. Wolfe et al.

Title Page

Abstract

Introduction

Conclusions

References

Tables

Figures

◀

▶

◀

▶

Back

Close

Full Screen / Esc

Printer-friendly Version

Interactive Discussion



Palmer et al., 2006, 2003), South America (Barkley et al., 2013, 2008), Europe (Curci et al., 2010; Dufour et al., 2009), Africa (Marais et al., 2012), Asia (Fu et al., 2007; Stavrakou et al., 2014), and globally (Fortems-Cheiney et al., 2012; Shim et al., 2005; Stavrakou et al., 2009). Future geostationary observations, such as the NASA Tropospheric Emissions: Monitoring of Pollution (TEMPO, <http://science.nasa.gov/missions/tempo/>) mission, will permit an even more detailed investigation of the spatial and temporal variability of isoprene emissions and other VOC sources.

Chemistry dictates the relationship between HCHO columns and underlying isoprene emissions. Many of the above-listed studies apply 0-D box model calculations to evaluate the yield of HCHO from isoprene as a function of oxidation time, NO_x regime and chemical mechanism. In all cases, it is found that NO_x enhances both the production rate and ultimate yield of HCHO. Slower production at lower NO_x can lead to “smearing,” whereby HCHO production is displaced relative to the isoprene source. Palmer et al. (2003) define a characteristic smearing length scale, which can range from 10 to 100 km or more. Furthermore, accumulation of oxygenated VOC over multiple generations of isoprene degradation can contribute to substantial background HCHO production, which is not directly linked with fresh isoprene emissions. Long-lived primary anthropogenic or biogenic emissions, like methane and methanol, can also contribute to this background. Background column concentrations are typically on the order of $5 \times 10^{15} \text{ cm}^{-2}$, equating to 20 % or more of the isoprene-driven HCHO column enhancement (Barkley et al., 2013; Millet et al., 2006). A wave of recent theoretical (Peeters et al., 1999, 2014; Peeters and Müller, 2010), laboratory (Crounse et al., 2012, 2011; Paulot et al., 2009a, b) and field (Mao et al., 2012) research has highlighted shortcomings in low-NO_x isoprene oxidation schemes. Such issues translate directly into top-down emission estimates; for example, Marais et al. (2012) report an uncertainty of 40 % in OMI-derived African isoprene emissions at high-NO_x and 40–90 % at low-NO_x. Coarse resolution of averaged satellite observations and model simulations (typically 1° × 1° or more) has partly mitigated these problems in prior work, as variability in NO_x-dependent smearing and background production is averaged out. A more care-

ful treatment will be needed to harness the enhanced resolution of near-future orbital observations (e.g., 8 km × 4.5 km for TEMPO), especially since these measurements will include diurnal variability.

Here, we use a comprehensive set of in situ observations to quantify the impact of NO_x on the isoprene-HCHO chemical link. Using isoprene and its unique first-generation products, we segregate HCHO into two categories. The first, defined as “prompt” HCHO, is produced from fresh isoprene emissions (on a timescale of less than a day) and retains the signature of isoprene emission source strength. The second category is “background” HCHO stemming from oxidation of longer-lived isoprene oxidation products and other VOC. We examine the NO_x dependence of both quantities. Applying the same method to 0-D and global model simulations, we evaluate the ability of current chemical mechanisms to replicate the observed trends. Box model results are also used to elucidate the mechanistic underpinnings of the NO_x influence on HCHO production.

2 SENEX observations

The Southeast Nexus (SENEX) mission was an airborne campaign designed to examine the interaction of natural and anthropogenic emissions. During June and July of 2013, the NOAA WP-3D aircraft logged 114 flight hours over 18 research flights in a range of environments throughout the Southeast United States, including urban centers, power plant plumes, natural gas extraction regions, agricultural areas and forests. The payload included a suite of gas- and particle-phase instrumentation (Warneke et al., 2015). Here we utilize observations of HCHO, isoprene, methyl vinyl ketone (MVK), methacrolein (MACR), NO and NO₂. HCHO was measured at 1 Hz by the NASA In Situ Airborne Formaldehyde (ISAF) instrument, which relies on the laser-induced fluorescence technique and has an accuracy of ±10% (Cazorla et al., 2015). Isoprene, MVK and MACR were measured by both a quadrupole proton transfer reaction mass spectrometer (PTR-MS) and the NOAA improved whole-air sampler (iWAS)

Formaldehyde production from isoprene oxidation across NO_x regimes

G. M. Wolfe et al.

Title Page

Abstract

Introduction

Conclusions

References

Tables

Figures



Back

Close

Full Screen / Esc

Printer-friendly Version

Interactive Discussion



**Formaldehyde
production from
isoprene oxidation
across NO_x regimes**

G. M. Wolfe et al.

[Title Page](#)[Abstract](#)[Introduction](#)[Conclusions](#)[References](#)[Tables](#)[Figures](#)[◀](#)[▶](#)[◀](#)[▶](#)[Back](#)[Close](#)[Full Screen / Esc](#)[Printer-friendly Version](#)[Interactive Discussion](#)

with offline gas chromatography. The PTR-MS (de Gouw and Warneke, 2007) has a stated accuracy of 20 % and sequentially sampled masses for isoprene ($m/z +69$) and the sum of MVK and MACR ($m/z +71$) for 1 s each with a duty cycle of 14 s. The iWAS (Lerner et al., 2015) collected 72 canister samples each flight, which were
5 analyzed offline with gas chromatography – mass spectrometry 3–4 days post-flight. iWAS measurement uncertainty is 20 % for speciated MVK and MACR and 27 % for isoprene. NO and NO₂ were measured at 1 Hz via chemiluminescence coupled with a photolytic NO₂ converter (Pollack et al., 2010; Ryerson et al., 1999) with an accuracy of 5 %. Data are filtered to include only daytime boundary layer conditions (solar
10 zenith angle < 60°, radar altitude < 1 km). Influence from biomass burning (acetonitrile > 210 pptv and CO > 300 ppbv) is also removed. This procedure, along with the disjoint nature of the PTR-MS measurement, excludes 50 % of all fast (1 Hz) data. After accounting for missing data, we retain 8435 1 Hz data points and 81 iWAS samples.

Measurements of MVK and MACR can include a positive bias from conversion of
15 isoprene hydroxyhydroperoxides (ISOPOOH) on hot metal surfaces in the sampling system (Liu et al., 2013; Rivera-Rios et al., 2014). Theoretically, this mechanism could give rise to an analogous artifact in HCHO observations. ISOPOOH mixing ratios of roughly 0 to 2 ppbv were observed during SENEX (see Supplement). It is difficult to quantify the magnitude of any such interference from field observations alone. Based
20 on a comparison to observations of other isoprene oxidation products and to 0-D box model results (Supplement), we argue that such artifacts are negligibly small in the PTR-MS and ISAF observations for SENEX. We cannot rule out a potential positive bias in the iWAS MVK measurement; nonetheless, as we show below, the correspondence between observed MVK and MACR mixing ratios is consistent with our current
25 understanding of isoprene oxidation.

SENEX sampled a wide spectrum of chemical regimes (Fig. 1). For the daytime boundary-layer observations presented here, maximum 1 Hz isoprene and NO mixing ratios respectively reach 8.1 and 95 ppbv, while minima are less than a few pptv. The distributions of both isoprene and NO observations are approximately log-normal (top

Formaldehyde production from isoprene oxidation across NO_x regimes

G. M. Wolfe et al.

Title Page

Abstract

Introduction

Conclusions

References

Tables

Figures



Back

Close

Full Screen / Esc

Printer-friendly Version

Interactive Discussion



and right panels of Fig. 1), peaking at 1.5 ppbv and 50 pptv, respectively. Though these distributions may be biased towards areas of urban influence, the range of environments encountered during SENEX is representative of the Southeast US summertime boundary layer. The long tail at the low end of the isoprene distribution is mostly associated with regions lacking significant tree cover, notably Illinois and Indiana, where isoprene emissions are lower. The NO distribution spans four orders of magnitude (< 10 to ~ 10⁴ pptv), over which radical chemistry changes markedly. At NO mixing ratios of a few hundred pptv or more, organic peroxy radicals (RO₂) react mostly with NO. At low NO (10's of pptv or less), reaction with HO₂, other RO₂ and isomerization dominate the RO₂ fate. The bulk of the NO distribution lies in a transition region for radical chemistry, making this dataset ideal for probing the anthropogenic influence on biogenic VOC oxidation.

HCHO mixing ratios (color shading in Fig. 1) range from 0.8 to 14 ppbv with a mean value of 4.3 ppbv. HCHO is most abundant in regions where both isoprene and NO_x are elevated. High NO_x is often accompanied by increased concentrations of anthropogenic VOC; however, constrained box-model calculations demonstrate that isoprene is the dominant HCHO precursor even in these cases (Sect. 5). Thus, chemistry (and not co-variance of NO_x and anthropogenic VOC) drives the observed NO_x dependence of HCHO abundance.

3 Linking observed and emitted isoprene

The isoprene photochemical cascade is a multi-step process. Isoprene oxidation is initiated by reaction with the hydroxyl radical (OH), ozone, or the nitrate radical (NO₃). In the Southeast US, typical daytime levels for OH, ozone and NO₃ are 4 × 10⁶ cm⁻³, 50 ppbv and 0.1 pptv, respectively (OH and NO₃ are estimated from median box model output, see Sect. 5). The corresponding isoprene lifetimes at 298 K are 0.7, 17 and 160 h, respectively. Thus, reaction with OH typically constitutes 95 % or more of the total daytime isoprene sink in this environment. Addition of OH and reaction with O₂

Formaldehyde production from isoprene oxidation across NO_x regimes

G. M. Wolfe et al.

Title Page

Abstract

Introduction

Conclusions

References

Tables

Figures

◀

▶

◀

▶

Back

Close

Full Screen / Esc

Printer-friendly Version

Interactive Discussion



generates one of several isoprene hydroxyperoxy radicals (ISOPO₂). ISOPO₂ isomers interconvert rapidly due to reversible O₂ addition (Peeters et al., 2009) but are eventually destroyed via reaction with NO, hydroperoxy radical (HO₂), other organic peroxy radicals (RO₂) or isomerization. Most branches have the potential to produce HCHO, with varying yields. The laboratory-derived first-generation HCHO yield from the NO pathway is ~ 0.6 (Atkinson and Arey, 2003), though this value may be less representative of the real atmosphere due to the very high isoprene concentrations (and very short RO₂ lifetimes) in early chamber experiments. The first-generation yield from the HO₂ pathway is ~ 0.06 (Liu et al., 2013). Isomerization chemistry is less well understood; the 1,5-H-shift is believed to produce HCHO with a unity yield, while the much faster 1,6-H-shift should not produce any HCHO (da Silva et al., 2010; Fuchs et al., 2013; Peeters et al., 2009, 2014; Peeters and Müller, 2010). Regardless of the specific pathway, MVK or MACR are always co-produced with HCHO in the first generation. HCHO is also generated in subsequent chemistry, but on a longer timescale and from a much larger suite of precursors. For example, the OH lifetimes of MACR and MVK are respectively 3.5 and 5 times longer than that of isoprene.

Boundary layer composition reflects a mixture of emissions with various degrees of photochemical processing. To isolate the impact of “fresh” isoprene emissions, we exploit the relatively simple chemistry of MVK and MACR, which are produced via isoprene oxidation and lost primarily via reaction with OH.



Rate constants (k) are taken from the IUPAC database (Atkinson et al., 2006). These reactions form the basis for a photochemical clock of isoprene oxidation (de Gouw et al., 2005; Roberts et al., 2006; Stroud et al., 2001). Integration of the kinetic equations for this system shows that the product/parent ratios are a function of the rate constants, yield (y), reaction time (t) and mean OH concentration. In the case of MACR,

for example:

$$\frac{[\text{MACR}]}{[\text{ISOP}]} = \frac{y_{\text{MACR}}k_1}{k_2 - k_1} (1 - \exp((k_1 - k_2)[\text{OH}]t)) \quad (1)$$

An analogous expression holds for MVK. As noted by Stroud et al. (2001), this “sequential reaction model” is purely chemical and does not account for the effects of mixing and transport. Indeed, this analysis relates daughter/parent ratios to an “average” photochemical age, when in fact there is a broad distribution of ages in any mixed air mass. We also implicitly assume that direct emissions (Fares et al., 2015) and deposition (Karl et al., 2010) of MVK and MACR do not significantly influence the budget of these compounds.

Two potential issues arise when applying this model to the real atmosphere. First, the yields of MVK and MACR are dependent on ISOPO₂ branching and are thus a non-linear function of NO_x. Previous applications of this method (de Gouw et al., 2005; Roberts et al., 2006; Stroud et al., 2001) have assumed lab-derived high-NO_x yields of 0.33 and 0.23 for MVK and MACR, respectively (Atkinson and Arey, 2003), but this may not be appropriate in the present case; furthermore, these yields are not fully consistent with current chemical mechanisms (Fig. S4 in the Supplement). We explicitly examine the effects of NO_x-varying yields below using yield curves derived from box model simulations (see Supplement for details). Second, the photochemical age (*t*) implied by any observed daughter/parent ratio depends on the concentration of OH, which was not measured and varies as an air mass ages. Rather than assume a single “typical” value for OH, we express photochemical age in terms of “exposure,” defined here as the product of OH concentration and reaction time averaged over the photochemical lifetime of an air mass.

Figure 2 compares the observed relationship of MVK/isoprene and MACR/isoprene ratios against theoretical trends predicted by the sequential reaction model. Theoretical ratios are calculated at fixed exposures of 2, 4, 8, 12 and 16 × 10⁶ OHcm⁻³h using two sets of yields: high NO (NO = 1000 pptv, *y*_{MVK} = 0.41, *y*_{MACR} = 0.28) and low

Formaldehyde production from isoprene oxidation across NO_x regimes

G. M. Wolfe et al.

Title Page

Abstract

Introduction

Conclusions

References

Tables

Figures



Back

Close

Full Screen / Esc

Printer-friendly Version

Interactive Discussion



Formaldehyde production from isoprene oxidation across NO_x regimes

G. M. Wolfe et al.

Title Page

Abstract

Introduction

Conclusions

References

Tables

Figures

◀

▶

◀

▶

Back

Close

Full Screen / Esc

Printer-friendly Version

Interactive Discussion

NO (NO = 50 pptv, $y_{\text{MVK}} = 0.21$, $y_{\text{MACR}} = 0.19$). Observed ratios of MVK/isoprene vs. MACR/isoprene exhibit a tight linear correlation. Higher ratios are often associated with higher NO_x, likely reflecting enhanced OH and higher product yields in these air masses. Far downwind from isoprene and NO_x source regions, we would expect to see higher MVK/isoprene and MACR/isoprene ratios associated with lower NO_x due to removal of the latter. The theoretical slope agrees well with observations, indicating exposures of 1–16 × 10⁶ OHcm⁻³h. For a typical daytime OH concentration of 4 × 10⁶ cm⁻³, this corresponds to processing times of 0.25–4 h.

The ratio of y_{MVK} to y_{MACR} dictates the location of the theoretical line and thus the correspondence between daughter/parent ratios and exposure. For example, a MACR/isoprene ratio of 1 would be consistent with an exposure of 4.9 × 10⁶ OHcm⁻³h at high-NO_x conditions (NO = 1000 pptv) vs. 6.1 × 10⁶ OHcm⁻³h at low-NO_x (NO = 50 pptv). Thus, for any given daughter/parent ratio, a higher assumed yield gives a smaller derived exposure. Observations in Fig. 2 fall above the high-NO_x theoretical relationship. As discussed in the Supplement, however, iWAS MVK measurement may contain a positive artifact on the order of 34–51 %. This potential systematic error (thick black line in Fig. 2) overlaps both the high and low-NO_x theoretical relationships. Given the wide range of conditions sampled, we elect to use a NO_x-dependent yield for MVK and MACR. For this purpose, model-derived yields (Fig. S4 and Supplement) are interpolated to observed NO mixing ratios.

We can effectively reverse this photochemical clock to derive a proxy for the total isoprene emissions that had been released into the sample air masses (de Gouw et al., 2005). First, we calculate OH exposures from observed daughter/parent ratios by inverting Eq. (1). To perform this calculation with PTR-MS data (which has far greater coverage), we partition the measured sum between MVK and MACR using MVK/MACR ratios from box model calculations (Sect. 5). Modeled MVK/MACR ratios (with an output interval of 1 min) are linearly interpolated to the 14 s observational time base. The MVK/MACR ratio does not vary dramatically (mean ± 1σ: 1.3 ± 0.2), and using a constant ratio instead alters results by less than 4 %. Calculated exposures

range from 0.5 to $18 \times 10^6 \text{ OH cm}^{-3} \text{ h}$ (Fig. S5a). Exposures derived from MACR are 6% higher than those from MVK on average, and we use the mean of these two values. Next, an “initial” isoprene mixing ratio, ISOP_0 , is estimated via reverse integration of isoprene’s first-order loss rate:

$$5 \quad [\text{ISOP}]_0 = [\text{ISOP}] \exp(k_1 [\text{OH}] t) \quad (2)$$

ISOP_0 represents the amount of isoprene that an air parcel would have to start with to generate the amount of isoprene, MVK and MACR observed. Thus, it is an observationally-constrained surrogate for isoprene emission strength (modulated to some degree by boundary layer height, as it is a volume-based quantity). ISOP_0 mixing ratios are typically 2–10 times higher than observed isoprene (Fig. S5b).

4 The yield of HCHO from isoprene

The definition of “yield” can vary with context and requires careful consideration when quantifying the chemical relationships. In a mechanistic sense, the “first generation yield” refers to the amount of HCHO produced per unit isoprene consumed in the first stage of oxidation. This is analogous to the yields of MVK and MACR used in the above calculation of initial isoprene. The model-derived first-generation HCHO yield from isoprene varies by more than a factor of 2 over the range of chemical environments encountered during SENEX (Fig. S4). An alternative definition is that of the “total yield” (sometimes referred to as the “molar yield,” e.g. Millet et al., 2006), a time-dependent quantity that describes the total amount of HCHO produced over multiple generations of oxidation. The total yield is typically derived from model simulations and used to relate satellite HCHO column observations to isoprene emissions (Marais et al., 2012; Millet et al., 2006). Early studies acknowledged the NO_x dependence of the total yield (Millet et al., 2006; Palmer et al., 2003), and more recent work has attempted to account for this dependence using NO_2 column observations (Marais et al., 2012). Here,

Formaldehyde production from isoprene oxidation across NO_x regimes

G. M. Wolfe et al.

Title Page

Abstract

Introduction

Conclusions

References

Tables

Figures



Back

Close

Full Screen / Esc

Printer-friendly Version

Interactive Discussion



Formaldehyde production from isoprene oxidation across NO_x regimes

G. M. Wolfe et al.

Title Page

Abstract

Introduction

Conclusions

References

Tables

Figures

◀

▶

◀

▶

Back

Close

Full Screen / Esc

Printer-friendly Version

Interactive Discussion



we define the “prompt yield” as the change in observed HCHO per unit change in ISOP_0 ($y_p = \Delta\text{HCHO}/\Delta\text{ISOP}_0$). This is not the same as the first-generation yield, since y_p can include HCHO production and loss over several hours (depending on the photochemical exposure of an air mass). Nor is it the same as the total yield, which inherently does not account for HCHO loss as an air mass ages. The prompt yield is effectively a quantity that relates isoprene emission strength to observed HCHO abundance. As we will demonstrate, y_p is well-suited for segregating the various drivers of HCHO and for benchmarking model performance.

Figure 3a shows the relationship between calculated ISOP_0 and observed HCHO. The overall correlation is linear with a striking NO_x gradient. To quantify this NO_x dependence, we sort the data by $\log(\text{NO}_x)$, group it into 20 bins such that each bin contains the same number of points ($N = 416$), and perform a major-axis linear fit of HCHO vs. ISOP_0 for each bin. Individual fits give r^2 values of 0.6–0.8, except for the highest NO_x bin ($r^2 = 0.48$) that contains some heavily-polluted air masses, such as downwind from power plants. Very fresh power plant plumes, defined as $\log(\text{NO}_x)$ values exceeding a mean $+3\sigma$ threshold, are removed prior to this procedure to avoid skewing the highest NO_x bin. Results are independent of the number of bins chosen or time resolution (e.g., 1 s vs. 1 min data).

The HCHO- ISOP_0 slope (Fig. 3b) represents the prompt yield. This yield varies by a factor of 3 over the range of observed NO_x , from 0.3 for NO_x mixing ratios of a few hundred pptv to 0.9 at $\text{NO}_x > 1$ ppbv. At low NO_x , y_p is comparable to the MCM-predicted direct first-generation yield of HCHO (0.3–0.4 at $\text{NO} = 10$ –40 pptv, Fig. S4), while at high NO_x it is somewhat higher than the predicted first-generation yield (0.74 at $\text{NO} = 1000$ pptv). This likely reflects the inclusion of more than one generation of HCHO production at higher NO_x , where oxidation is more rapid (median exposures increase by 38 % over the range of observed NO_x values). Most of this portion of the HCHO budget, however, stems from first-generation production.

The intercept (Fig. 3c) represents the abundance of “background” HCHO. This portion of the HCHO budget stems mainly from air that either has not encountered strong

**Formaldehyde
production from
isoprene oxidation
across NO_x regimes**

G. M. Wolfe et al.

Title Page

Abstract

Introduction

Conclusions

References

Tables

Figures

◀

▶

◀

▶

Back

Close

Full Screen / Esc

Printer-friendly Version

Interactive Discussion



isoprene emissions or is so aged that most of the isoprene has reacted away and can no longer be linked to a specific source region. Some of this background may also stem from oxidation of long-lived primary emissions like methane or methanol. Box model calculations (Sect. 5) indicate average HCHO budget contributions of 0.3 ± 0.2 ppbv and 0.2 ± 0.1 ppbv from methane and methanol, respectively. Background HCHO also exhibits a marked NO_x dependence, increasing from 1.6 to 3.3 ppbv over the observed NO_x range. As with y_p, we expect such behavior since NO_x regulates the fate of all organic peroxy radicals (see Sect. 6). Assuming a 1 km mixed layer depth (Wagner et al., 2015), the corresponding HCHO column density for this background is $4\text{--}8 \times 10^{15} \text{ cm}^{-2}$. This is comparable to the background reported by previous investigations of satellite-derived HCHO columns (Barkley et al., 2013; Millet et al., 2006). None of these studies explicitly account for the NO_x dependence of the background, though it can represent a substantial fraction of the total HCHO column – maximum summertime HCHO columns over the southeast US are $\sim 25 \times 10^{15} \text{ cm}^{-2}$ (Millet et al., 2008). Given the strong NO_x dependence of both y_p and background HCHO, grouping HCHO column observations by NO_x (e.g. using simultaneous observations of NO₂ columns (Marais et al., 2012) or model-derived NO_x) and performing an analysis similar to that described here should provide a robust means of accounting for these influences.

5 Model evaluation

Next, we compare the observed HCHO-ISOP₀ relationship to results from a global chemical-transport model and a 0-D box model. Our goals are to both illustrate the utility of this analysis and evaluate model performance. By going beyond a simple comparison of modeled and measured mixing ratios, we can more accurately pinpoint potential shortcomings in model chemistry.

The GFDL AM3 model is an atmospheric general circulation model with interactive chemistry (Donner et al., 2011), including recent updates to the representation of isoprene degradation (Mao et al., 2013; Naik et al., 2013). Model simulations were carried

out at 50 km × 50 km resolution with horizontal winds nudged to NCEP GFS analyses and sampled along the SENEX flight tracks at a time resolution of 1 min. Further details are available elsewhere (Li et al., 2015).

The University of Washington Chemical Box Model (UWCM v2.2) is a versatile 0-dimensional framework for simulating various chemical systems, including lab chamber experiments (Wolfe et al., 2012) and observations from ground (Kim et al., 2015, 2013; Wolfe et al., 2014) and airborne (Marvin et al., 2015) platforms. Multiple chemical mechanisms are available within UWCM; here we used the latest version of the Master Chemical Mechanism (MCM v3.3, Jenkin et al., 2015). UWCM was constrained with 1 min average observations of isoprene, NO₂, ozone, CO, PAN, methane, methanol and meteorology and assumed clear-sky conditions for photolysis frequencies. The chemical system was integrated forward in time to diel steady state (total integration time of 3 days) for each set of measurements. This setup inherently assumes that the atmosphere is in chemical steady state – that is, that production and loss of HCHO, MVK, MACR and other species are roughly balanced. This assumption is rarely strictly true and may fail for highly-aged air masses (where isoprene is depleted) or close to strong local emissions. Nonetheless, it is a fair approximation for the daytime well-mixed boundary layer observations that prevailed during SENEX. Monoterpenes and anthropogenic VOC are excluded from the simulation since observations of these species (from the iWAS) are relatively sparse. Separate sensitivity simulations utilizing the iWAS data suggest that observed monoterpenes and anthropogenic VOC (a subset of alkanes, alkenes and aromatics) increase modeled HCHO by 1 ± 2 % and 2 ± 3 %, respectively. A more detailed evaluation of box model performance is forthcoming (Marvin et al., 2015).

Output from both models is filtered for daytime, boundary-layer, non-biomass burning points using the same criteria as that for observations (Sect. 2). Both models adequately reproduce observed HCHO mixing ratios (Fig. S6). We perform the same analyses as described above to derive model y_p and background HCHO. Because of the reduced time resolution, we group results into 10 NO_x bins, instead of 20, before

**Formaldehyde
production from
isoprene oxidation
across NO_x regimes**

G. M. Wolfe et al.

Title Page

Abstract

Introduction

Conclusions

References

Tables

Figures

◀

▶

◀

▶

Back

Close

Full Screen / Esc

Printer-friendly Version

Interactive Discussion



creasing NO enhances the conversion of HO₂ to OH (Reaction R4) and thus accelerates VOC oxidation (Reaction R5) and HCHO loss. Subsequent production of HCHO depends on the structure and fate of RO₂ intermediates, which can react with NO, HO₂, other RO₂, or isomerize (Reaction R6).



Here, α represents a bulk branching ratio for HCHO production weighted over all RO₂ reactions. The RO₂ lifetime is typically less than 100 s during the day, so Reaction (R5) is the rate-limiting step in HCHO formation. The HCHO production rate is then equal to the product of the total RO₂ production rate and the bulk branching ratio.

To disentangle these factors, we extract chemical rates from the diel steady-state UWCM simulations discussed in Sect. 5. Figure 5 shows the gross production rates for total peroxy radicals and HCHO as a function of NO_x. Consistent with our earlier discussion, total HCHO production increases by more than a factor of 3 from low to high NO_x. In contrast, RO₂ production is effectively constant within model variability. Closer scrutiny reveals that a factor of 3–4 increase in OH concentrations between low and high NO_x is more than offset by a concomitant reduction in isoprene (results not shown). The ratio of HCHO to RO₂ production rates gives an estimate for α, which increases from 0.14 to 0.39 across this NO_x range (Fig. 5). Though the total RO₂ production rate includes reactions that do not make HCHO, α is still a useful metric for the relationship between HCHO production and overall VOC oxidation. Based on this analysis, we conclude that changes in RO₂ branching are the dominant factor driving the NO_x dependence of HCHO production and abundance.

25 Increased OH also reduces the lifetime of HCHO, which may affect the HCHO budget if this reaction becomes competitive with photolysis. UWCM predicts an average HCHO photolysis lifetime of 4 h and OH reaction lifetimes that range from 3 h at high NO_x to 12 h at low NO_x. Thus, photolysis is typically the dominant loss process and the scaling

**Formaldehyde
production from
isoprene oxidation
across NO_x regimes**

G. M. Wolfe et al.

Title Page

Abstract

Introduction

Conclusions

References

Tables

Figures



Back

Close

Full Screen / Esc

Printer-friendly Version

Interactive Discussion



of HCHO lifetime with OH is typically weak. As a result, the net chemical tendency of HCHO (production minus loss) is positive and increasing throughout the range of model NO_x conditions. Faster loss due to reaction with OH therefore only slightly dampens the enhancement in HCHO production.

7 Conclusions

Using SENEX aircraft observations, we have quantified the NO_x dependence of the relationship between isoprene emission strength and HCHO mixing ratios. Simultaneous measurements of isoprene, MVK and MACR define a photochemical clock for isoprene oxidation, allowing separation of prompt HCHO production (which retains the isoprene source signature) and background HCHO from late-generation isoprene oxidation products, methane and other long-lived VOC. The prompt HCHO yield increases by a factor of 3 (0.3 to 0.9 ppbv ppbv⁻¹) and the average background HCHO mixing ratio more than doubles (1.6 to 3.3 ppbv) over the range of NO_x values encountered in the southeast US. This analytical method is applied to evaluate the performance of a global chemical transport model and a 0-D box model. Both models accurately reproduce the observed NO_x trend of the prompt HCHO yield, indicating that both chemical mechanisms accurately capture early-stage isoprene oxidation. On the other hand, both models also under-predict background HCHO abundance by 0.5 – 1 ppbv, which can be a significant fraction of total HCHO in some cases. This may suggest insufficient build-up of isoprene-derived long-lived precursors in the models, missing VOC not related to isoprene, or insufficient OH. Box model results also provide insight into the mechanistic drivers of the observed NO_x trends. We find that increasing NO_x does not significantly affect total RO_2 production due to the cancelling effects of higher OH and lower VOC. Thus, the positive correlation between NO_x and HCHO primarily reflects the changing fate of RO_2 radicals.

To our knowledge, there are no direct laboratory measurements of HCHO yields from low- NO_x isoprene chemistry; thus, the results presented here constitute the first

Formaldehyde production from isoprene oxidation across NO_x regimes

G. M. Wolfe et al.

Title Page

Abstract

Introduction

Conclusions

References

Tables

Figures

⏪

⏩

◀

▶

Back

Close

Full Screen / Esc

Printer-friendly Version

Interactive Discussion



**Formaldehyde
production from
isoprene oxidation
across NO_x regimes**

G. M. Wolfe et al.

Title Page

Abstract

Introduction

Conclusions

References

Tables

Figures



Back

Close

Full Screen / Esc

Printer-friendly Version

Interactive Discussion



measurement-constrained evaluation of the isoprene-HCHO link across NO_x regimes. The AM3 and MCMv3.3 mechanisms differ substantially (the former is highly condensed while the latter is explicit), but both contain recent updates to isoprene degradation. We expect that other mechanisms will also perform well if they accurately reflect our current best understanding. The observations presented here do not include the extremely-low NO_x regime (NO_x < 0.1 ppbv) typical of remote regions like the Amazon and equatorial Africa. In such pristine regions, smearing of HCHO production is expected to be more severe (Barkley et al., 2013), and total HCHO production may be significantly lower if the RO₂ fate favors functionalization over fragmentation (e.g. isomerization). More work is needed to map out this area of the urban-rural spectrum. It may also be possible to apply the methods developed here to evaluate the chemistry of glyoxal, another key tracer of VOC oxidation that is also amenable to orbital observations (Kaiser et al., 2015b; Li et al., 2015) and is believed to be an important precursor for SOA (McNeill et al., 2012).

These results also carry implications for top-down isoprene emission estimates. Uncertainties in low-NO_x chemistry are often cited as the largest source of potential error in derived emissions (Marais et al., 2012; Palmer et al., 2006). Based on our analysis, current mechanisms appear to capture low-NO_x production of HCHO, MVK and MACR, thus such errors are likely less severe than commonly asserted. Recent work has acknowledged the impact of NO_x on the prompt yield of HCHO from isoprene (Marais et al., 2012). We advocate considering the NO_x dependence of background HCHO as well, since this can constitute a significant fraction of the total HCHO column. For scale, the derived background HCHO mixing ratio of 1.6–3.3 ppbv is 37–77 % of the campaign-mean observed HCHO mixing ratio of 4.3 ppbv. Forthcoming geostationary observations will resolve local gradients in chemical regime, and smearing and background HCHO production will become problematic even in high-NO_x regions. Indeed, even current-generation orbital instruments are capable of resolving some urban-rural gradients in HCHO columns (Boeke et al., 2011). When applying advanced statistical techniques like inversion, model results will only be as accurate as the chemical mech-

anisms driving them. Continued field observations are crucial for providing confidence in our ability to link HCHO to its sources.

Data availability

All data used in this study are publicly accessible on the SENEX website (<http://www.esrl.noaa.gov/csd/projects/senex/>).

The Supplement related to this article is available online at doi:10.5194/acpd-15-31587-2015-supplement.

Acknowledgements. We are grateful to NOAA AOC and the flight crew of the WP-3D for enabling a super awesome mission. HCHO measurement efforts were supported by US EPA Science to Achieve Results (STAR) program grant 83540601 and NASA grant NNX14ZDA001N-SEAC4RS. Analysis was supported by NASA ACCDAM grant NNX14AP48G. J. Kaiser acknowledges support from NASA ESSF grant NNX14AK97H. C. D. Hatch was supported by the Hendrix faculty grant and the Hendrix College Odyssey program. J. Mao and L. W. Horowitz acknowledge support from NOAA Climate Program Office grant # NA13OAR4310071. This research has not been subjected to any EPA review and therefore does not necessarily reflect the views of the agency, and no official endorsement should be inferred.

References

Abbot, D. S., Palmer, P. I., Martin, R. V., Chance, K. V., Jacob, D. J., and Guenther, A.: Seasonal and interannual variability of North American isoprene emissions as determined by formaldehyde column measurements from space, *Geophys. Res. Lett.*, 30, 1886, doi:10.1029/2003GL017336, 2003.

Atkinson, R. and Arey, J.: Gas-phase tropospheric chemistry of biogenic volatile organic compounds: a review, *Atmos. Environ.*, 37, S197–S219, 2003.

Formaldehyde production from isoprene oxidation across NO_x regimes

G. M. Wolfe et al.

Title Page

Abstract

Introduction

Conclusions

References

Tables

Figures



Back

Close

Full Screen / Esc

Printer-friendly Version

Interactive Discussion



**Formaldehyde
production from
isoprene oxidation
across NO_x regimes**

G. M. Wolfe et al.

Title Page

Abstract

Introduction

Conclusions

References

Tables

Figures



Back

Close

Full Screen / Esc

Printer-friendly Version

Interactive Discussion



Atkinson, R., Baulch, D. L., Cox, R. A., Crowley, J. N., Hampson, R. F., Hynes, R. G., Jenkin, M. E., Rossi, M. J., Troe, J., and IUPAC Subcommittee: Evaluated kinetic and photochemical data for atmospheric chemistry: Volume II – gas phase reactions of organic species, *Atmos. Chem. Phys.*, 6, 3625–4055, doi:10.5194/acp-6-3625-2006, 2006.

5 Barkley, M. P., Palmer, P. I., Kuhn, U., Kesselmeier, J., Chance, K., Kurosu, T. P., Martin, R. V., Helmig, D., and Guenther, A.: Net ecosystem fluxes of isoprene over tropical South America inferred from Global Ozone Monitoring Experiment (GOME) observations of HCHO columns, *J. Geophys. Res.*, 113, D20304, doi:10.1029/2008JD009863, 2008.

10 Barkley, M. P., De Smedt, I., Van Roozendaal, M., Kurosu, T. P., Chance, K., Arneth, A., Hagerberg, D., Guenther, A., Paulot, F., Marais, E., and Mao, J. Q.: Top-down isoprene emissions over tropical South America inferred from SCIAMACHY and OMI formaldehyde columns, *J. Geophys. Res.-Atmos.*, 118, 6849–6868, doi:10.1002/jgrd.50552, 2013.

15 Boeke, N. L., Marshall, J. D., Alvarez, S., Chance, K. V., Fried, A., Kurosu, T. P., Rappengluck, B., Richter, D., Walega, J., Weibring, P., and Millet, D. B.: Formaldehyde columns from the Ozone Monitoring Instrument: urban versus background levels and evaluation using aircraft data and a global model, *J. Geophys. Res.-Atmos.*, 116, D05303, doi:10.1029/2010jd014870, 2011.

20 Carlton, A. and Baker, K.: Photochemical modeling of the Ozark Isoprene Volcano: MEGAN, BEIS, and their impacts on air quality predictions, *Environ. Sci. Technol.*, 45, 4438–4445, doi:10.1021/es200050x, 2011.

Cazorla, M., Wolfe, G. M., Bailey, S. A., Swanson, A. K., Arkinson, H. L., and Hanisco, T. F.: A new airborne laser-induced fluorescence instrument for in situ detection of formaldehyde throughout the troposphere and lower stratosphere, *Atmos. Meas. Tech.*, 8, 541–552, doi:10.5194/amt-8-541-2015, 2015.

25 Crouse, J. D., Paulot, F., Kjaergaard, H. G., and Wennberg, P. O.: Peroxy radical isomerization in the oxidation of isoprene, *Phys. Chem. Chem. Phys.*, 13, 13607–13613, 2011.

Crouse, J. D., Knap, H. C., Ørnsø, K. B., Jørgensen, S., Paulot, F., Kjaergaard, H. G., and Wennberg, P. O.: On the atmospheric fate of methacrolein: 1. Peroxy radical isomerization following addition of OH and O₂, *J. Phys. Chem. A*, 116, 5756–5762, doi:10.1021/jp211560u, 2012.

30 Curci, G., Palmer, P. I., Kurosu, T. P., Chance, K., and Visconti, G.: Estimating European volatile organic compound emissions using satellite observations of formaldehyde from the Ozone

**Formaldehyde
production from
isoprene oxidation
across NO_x regimes**

G. M. Wolfe et al.

Title Page

Abstract

Introduction

Conclusions

References

Tables

Figures



Back

Close

Full Screen / Esc

Printer-friendly Version

Interactive Discussion



Monitoring Instrument, Atmos. Chem. Phys., 10, 11501–11517, doi:10.5194/acp-10-11501-2010, 2010.

da Silva, G., Graham, C., and Wang, Z. F.: Unimolecular beta-hydroxyperoxy radical decomposition with OH recycling in the photochemical oxidation of isoprene, Env. Sci. Technol., 44, 250–256, 2010.

de Gouw, J. and Warneke, C.: Measurements of volatile organic compounds in the earths atmosphere using proton-transfer-reaction mass spectrometry, Mass Spectrom. Rev., 26, 223–257, doi:10.1002/mas.20119, 2007.

de Gouw, J. A., Middlebrook, A. M., Warneke, C., Goldan, P. D., Kuster, W. C., Roberts, J. M., Fehsenfeld, F. C., Worsnop, D. R., Canagaratna, M. R., Pszenny, A. A. P., Keene, W. C., Marchewka, M., Bertman, S. B., and Bates, T. S.: Budget of organic carbon in a polluted atmosphere: results from the New England Air Quality Study in 2002, J. Geophys. Res., 110, D16305, doi:10.1029/2004jd005623, 2005.

de Gouw, J. A., McKeen, S. A., Aikin, K. C., Brock, C. A., Brown, S. S., Gilman, J. B., Graus, M., Hanisco, T., Holloway, J. S., Kaiser, J., Keutsch, F. N., Lerner, B. M., Liao, J., Markovic, M. Z., Middlebrook, A. M., Min, K. E., Neuman, J. A., Nowak, J. B., Peischl, J., Pollack, I. B., Roberts, J. M., Ryerson, T. B., Trainer, M., Veres, P. R., Warneke, C., Welti, A., and Wolfe, G. M.: Airborne measurements of the atmospheric emissions from a fuel ethanol refinery, J. Geophys. Res.-Atmos., 120, 4385–4397, doi:10.1002/2015jd023138, 2015.

DiGangi, J. P., Boyle, E. S., Karl, T., Harley, P., Turnipseed, A., Kim, S., Cantrell, C., Maudlin III, R. L., Zheng, W., Flocke, F., Hall, S. R., Ullmann, K., Nakashima, Y., Paul, J. B., Wolfe, G. M., Desai, A. R., Kajii, Y., Guenther, A., and Keutsch, F. N.: First direct measurements of formaldehyde flux via eddy covariance: implications for missing in-canopy formaldehyde sources, Atmos. Chem. Phys., 11, 10565–10578, doi:10.5194/acp-11-10565-2011, 2011.

Donner, L. J., Wyman, B. L., Hemler, R. S., Horowitz, L. W., Ming, Y., Zhao, M., Golaz, J.-C., Ginoux, P., Lin, S. J., Schwarzkopf, M. D., Austin, J., Alaka, G., Cooke, W. F., Delworth, T. L., Freidenreich, S. M., Gordon, C. T., Griffies, S. M., Held, I. M., Hurlin, W. J., Klein, S. A., Knutson, T. R., Langenhorst, A. R., Lee, H.-C., Lin, Y., Magi, B. I., Malyshev, S. L., Milly, P. C. D., Naik, V., Nath, M. J., Pincus, R., Ploshay, J. J., Ramaswamy, V., Seman, C. J., Shevliakova, E., Sirutis, J. J., Stern, W. F., Stouffer, R. J., Wilson, R. J., Winton, M., Wittenberg, A. T., and Zeng, F.: The dynamical core, physical parameterizations, and basic simula-

**Formaldehyde
production from
isoprene oxidation
across NO_x regimes**

G. M. Wolfe et al.

Title Page

Abstract

Introduction

Conclusions

References

Tables

Figures



Back

Close

Full Screen / Esc

Printer-friendly Version

Interactive Discussion



tion characteristics of the atmospheric component AM3 of the GFDL Global Coupled Model CM3, *J. Climate*, 24, 3484–3519, doi:10.1175/2011jcli3955.1, 2011.

Dufour, G., Wittrock, F., Camredon, M., Beekmann, M., Richter, A., Aumont, B., and Burrows, J. P.: SCIAMACHY formaldehyde observations: constraint for isoprene emission estimates over Europe?, *Atmos. Chem. Phys.*, 9, 1647–1664, doi:10.5194/acp-9-1647-2009, 2009.

Fares, S., Paoletti, E., Loreto, F., and Brilli, F.: Bidirectional flux of methyl vinyl ketone and methacrolein in trees with different isoprenoid emission under realistic ambient concentrations, *Environ. Sci. Technol.*, 49, 7735–7742, doi:10.1021/acs.est.5b00673, 2015.

Fortems-Cheiney, A., Chevallier, F., Pison, I., Bousquet, P., Saunois, M., Szopa, S., Cressot, C., Kurosu, T. P., Chance, K., and Fried, A.: The formaldehyde budget as seen by a global-scale multi-constraint and multi-species inversion system, *Atmos. Chem. Phys.*, 12, 6699–6721, doi:10.5194/acp-12-6699-2012, 2012.

Fu, T. M., Jacob, D. J., Palmer, P. I., Chance, K., Wang, Y. X. X., Barletta, B., Blake, D. R., Stanton, J. C., and Pilling, M. J.: Space-based formaldehyde measurements as constraints on volatile organic compound emissions in east and south Asia and implications for ozone, *J. Geophys. Res. Atmos.*, 112, D06312, doi:10.1029/2006jd007853, 2007.

Fuchs, H., Hofzumahaus, A., Rohrer, F., Bohn, B., Brauers, T., Dorn, H., Haseler, R., Holland, F., Kaminski, M., Li, X., Lu, K., Nehr, S., Tillmann, R., Wegener, R., and Wahner, A.: Experimental evidence for efficient hydroxyl radical regeneration in isoprene oxidation, *Nature Geosci.*, 6, 1023–1026, doi:10.1038/NGEO1964, 2013.

Guenther, A. B., Jiang, X., Heald, C. L., Sakulyanontvittaya, T., Duhl, T., Emmons, L. K., and Wang, X.: The Model of Emissions of Gases and Aerosols from Nature version 2.1 (MEGAN2.1): an extended and updated framework for modeling biogenic emissions, *Geosci. Model Dev.*, 5, 1471–1492, doi:10.5194/gmd-5-1471-2012, 2012.

Hogrefe, C., Isukapalli, S. S., Tang, X. G., Georgopoulos, P. G., He, S., Zalewsky, E. E., Hao, W., Ku, J. Y., Key, T., and Sistla, G.: Impact of biogenic emission uncertainties on the simulated response of ozone and fine particulate matter to anthropogenic emission reductions, *J. Air Waste Man. Assoc.*, 61, 92–108, doi:10.3155/1047-3289.61.1.92, 2011.

Jenkin, M. E., Young, J. C., and Rickard, A. R.: The MCM v3.3.1 degradation scheme for isoprene, *Atmos. Chem. Phys.*, 15, 11433–11459, doi:10.5194/acp-15-11433-2015, 2015.

Kaiser, J., Wolfe, G. M., Bohn, B., Broch, S., Fuchs, H., Ganzeveld, L. N., Gomm, S., Häseler, R., Hofzumahaus, A., Holland, F., Jäger, J., Li, X., Lohse, I., Lu, K., Prévôt, A. S. H.,

**Formaldehyde
production from
isoprene oxidation
across NO_x regimes**

G. M. Wolfe et al.

Title Page

Abstract

Introduction

Conclusions

References

Tables

Figures



Back

Close

Full Screen / Esc

Printer-friendly Version

Interactive Discussion



Rohrer, F., Wegener, R., Wolf, R., Mentel, T. F., Kiendler-Scharr, A., Wahner, A., and Keutsch, F. N.: Evidence for an unidentified non-photochemical ground-level source of formaldehyde in the Po Valley with potential implications for ozone production, *Atmos. Chem. Phys.*, 15, 1289–1298, doi:10.5194/acp-15-1289-2015, 2015a.

5 Kaiser, J., Wolfe, G. M., Min, K. E., Brown, S. S., Miller, C. C., Jacob, D. J., deGouw, J. A., Graus, M., Hanisco, T. F., Holloway, J., Peischl, J., Pollack, I. B., Ryerson, T. B., Warneke, C., Washenfelder, R. A., and Keutsch, F. N.: Reassessing the ratio of glyoxal to formaldehyde as an indicator of hydrocarbon precursor speciation, *Atmos. Chem. Phys.*, 15, 7571–7583, doi:10.5194/acp-15-7571-2015, 2015b.

10 Karl, T., Harley, P., Emmons, L., Thornton, B., Guenther, A., Basu, C., Turnipseed, A., and Jardine, K.: Efficient atmospheric cleansing of oxidized organic trace gases by vegetation, *Science*, 330, 816–819, doi:10.1126/science.1192534, 2010.

Kefauver, S. C., Filella, I., and Peñuelas, J.: Remote sensing of atmospheric biogenic volatile organic compounds (BVOCs) via satellite-based formaldehyde vertical column assessments, *Int. J. Remote Sens.*, 35, 7519–7542, doi:10.1080/01431161.2014.968690, 2014.

15 Kim, S., Wolfe, G. M., Mauldin, L., Cantrell, C., Guenther, A., Karl, T., Turnipseed, A., Greenberg, J., Hall, S. R., Ullmann, K., Apel, E., Hornbrook, R., Kajii, Y., Nakashima, Y., Keutsch, F. N., DiGangi, J. P., Henry, S. B., Kaser, L., Schnitzhofer, R., Graus, M., Hansel, A., Zheng, W., and Flocke, F. F.: Evaluation of HO_x sources and cycling using measurement-constrained model calculations in a 2-methyl-3-butene-2-ol (MBO) and monoterpene (MT) dominated ecosystem, *Atmos. Chem. Phys.*, 13, 2031–2044, doi:10.5194/acp-13-2031-2013, 2013.

20 Kim, S., Kim, S.-Y., Lee, M., Shim, H., Wolfe, G. M., Guenther, A. B., He, A., Hong, Y., and Han, J.: Impact of isoprene and HONO chemistry on ozone and OVOC formation in a semirural South Korean forest, *Atmos. Chem. Phys.*, 15, 4357–4371, doi:10.5194/acp-15-4357-2015, 2015.

25 Knighton, W. B., Herndon, S. C., Franklin, J. F., Wood, E. C., Wormhoudt, J., Brooks, W., Fortner, E. C., and Allen, D. T.: Direct measurement of volatile organic compound emissions from industrial flares using real-time online techniques: proton Transfer Reaction Mass Spectrometry and Tunable Infrared Laser Differential Absorption Spectroscopy, *Ind. Eng. Chem. Res.*, 51, 12674–12684, doi:10.1021/ie202695v, 2012.

**Formaldehyde
production from
isoprene oxidation
across NO_x regimes**

G. M. Wolfe et al.

Title Page

Abstract

Introduction

Conclusions

References

Tables

Figures



Back

Close

Full Screen / Esc

Printer-friendly Version

Interactive Discussion

- Lee, M., Heikes, B. G., Jacob, D. J., Sachse, G., and Anderson, B.: Hydrogen peroxide, organic hydroperoxide, and formaldehyde as primary pollutants from biomass burning, *J. Geophys. Res.-Atmos.*, 102, 1301–1309, doi:10.1029/96jd01709, 1997.
- Lerner, B. M., Gilman, J. B., Kuster, W., and de Gouw, J. A. et al.: An improved, automated whole-air sampler and VOC GC-MS analysis system, in preparation, 2015.
- Li, J., Mao, J., Min, K. E., Washenfelder, R. A., Brown, S. S., Kaiser, J., Keutsch, F. N., Wolfe, G. M., Hanisco, T. F., Pollack, I. B., Ryerson, T. B., Graus, M., Gilman, J. B., Lerner, B. M., Warneke, C., de Gouw, J. A., Brock, C. A., Middlebrook, A. M., Henderson, B. H., Naik, V., Paulot, F., and Horowitz, L. W.: Observational constraints on glyoxal production from isoprene oxidation and its contribution to organic aerosol over the Southeast United States, in preparation, 2015.
- Liu, Y. J., Herdinger-Blatt, I., McKinney, K. A., and Martin, S. T.: Production of methyl vinyl ketone and methacrolein via the hydroperoxyl pathway of isoprene oxidation, *Atmos. Chem. Phys.*, 13, 5715–5730, doi:10.5194/acp-13-5715-2013, 2013.
- Luecken, D. J., Hutzell, W. T., Strum, M. L., and Pouliot, G. A.: Regional sources of atmospheric formaldehyde and acetaldehyde, and implications for atmospheric modeling, *Atmos. Environ.*, 47, 477–490, doi:10.1016/j.atmosenv.2011.10.005, 2012.
- Mao, J., Ren, X., Zhang, L., Van Duin, D. M., Cohen, R. C., Park, J.-H., Goldstein, A. H., Paulot, F., Beaver, M. R., Crounse, J. D., Wennberg, P. O., DiGangi, J. P., Henry, S. B., Keutsch, F. N., Park, C., Schade, G. W., Wolfe, G. M., Thornton, J. A., and Brune, W. H.: Insights into hydroxyl measurements and atmospheric oxidation in a California forest, *Atmos. Chem. Phys.*, 12, 8009–8020, doi:10.5194/acp-12-8009-2012, 2012.
- Mao, J., Horowitz, L. W., Naik, V., Fan, S., Liu, J., and Fiore, A. M.: Sensitivity of tropospheric oxidants to biomass burning emissions: implications for radiative forcing, *Geophys. Res. Lett.*, 40, 1241–1246, doi:10.1002/grl.50210, 2013.
- Marais, E. A., Jacob, D. J., Kurosu, T. P., Chance, K., Murphy, J. G., Reeves, C., Mills, G., Casadio, S., Millet, D. B., Barkley, M. P., Paulot, F., and Mao, J.: Isoprene emissions in Africa inferred from OMI observations of formaldehyde columns, *Atmos. Chem. Phys.*, 12, 6219–6235, doi:10.5194/acp-12-6219-2012, 2012.
- Marvin, M., Wolfe, G. M., and Salawitch, R., et al.: Evaluating mechanisms for isoprene oxidation using a constrained chemical box model and SENEX observations of formaldehyde, in preparation, 2015.

**Formaldehyde
production from
isoprene oxidation
across NO_x regimes**

G. M. Wolfe et al.

Title Page

Abstract

Introduction

Conclusions

References

Tables

Figures



Back

Close

Full Screen / Esc

Printer-friendly Version

Interactive Discussion



- McNeill, V. F., Woo, J. L., Kim, D. D., Schwier, A. N., Wannell, N. J., Sumner, A. J., and Barakat, J. M.: Aqueous-phase secondary organic aerosol and organosulfate formation in atmospheric aerosols: a modeling study, *Env. Sci. Technol.*, 46, 8075–8081, doi:10.1021/es3002986, 2012.
- 5 Millet, D. B., Jacob, D. J., Turquety, S., Hudman, R. C., Wu, S. L., Fried, A., Walega, J., Heikes, B. G., Blake, D. R., Singh, H. B., Anderson, B. E., and Clarke, A. D.: Formaldehyde distribution over North America: implications for satellite retrievals of formaldehyde columns and isoprene emission, *J. Geophys. Res.-Atmos.*, 111, D24S02, doi:10.1029/2005jd006853, 2006.
- 10 Millet, D. B., Jacob, D. J., Boersma, K. F., Fu, T. M., Kurosu, T. P., Chance, K., Heald, C. L., and Guenther, A.: Spatial distribution of isoprene emissions from North America derived from formaldehyde column measurements by the OMI satellite sensor, *J. Geophys. Res.-Atmos.*, 113, D02307, doi:10.1029/2007jd008950, 2008.
- Naik, V., Horowitz, L. W., Fiore, A. M., Ginoux, P., Mao, J., Aghedo, A. M., and Levy II, H.: Impact of preindustrial to present-day changes in short-lived pollutant emissions on atmospheric composition and climate forcing, *J. Geophys. Res.-Atmos.*, 118, 8086–8110, doi:10.1002/jgrd.50608, 2013.
- Palmer, P. I., Jacob, D. J., Fiore, A. M., Martin, R. V., Chance, K., and Kurosu, T. P.: Mapping isoprene emissions over North America using formaldehyde column observations from space, *J. Geophys. Res.-Atmos.*, 108, 4180, doi:10.1029/2002jd002153, 2003.
- 20 Palmer, P. I., Abbot, D. S., Fu, T. M., Jacob, D. J., Chance, K., Kurosu, T. P., Guenther, A., Wiedinmyer, C., Stanton, J. C., Pilling, M. J., Pressley, S. N., Lamb, B., and Sumner, A. L.: Quantifying the seasonal and interannual variability of North American isoprene emissions using satellite observations of the formaldehyde column, *J. Geophys. Res.-Atmos.*, 111, D12315, doi:10.1029/2005jd006689, 2006.
- Paulot, F., Crouse, J. D., Kjaergaard, H. G., Kroll, J. H., Seinfeld, J. H., and Wennberg, P. O.: Isoprene photooxidation: new insights into the production of acids and organic nitrates, *Atmos. Chem. Phys.*, 9, 1479–1501, doi:10.5194/acp-9-1479-2009, 2009a.
- 25 Paulot, F., Crouse, J. D., Kjaergaard, H. G., Kurten, A., St Clair, J. M., Seinfeld, J. H., and Wennberg, P. O.: Unexpected epoxide formation in the gas-phase photooxidation of isoprene, *Science*, 325, 730–733, doi:10.1126/science.1172910, 2009b.
- 30

**Formaldehyde
production from
isoprene oxidation
across NO_x regimes**

G. M. Wolfe et al.

Title Page

Abstract

Introduction

Conclusions

References

Tables

Figures



Back

Close

Full Screen / Esc

Printer-friendly Version

Interactive Discussion



Peeters, J. and Müller, J. F.: HO_x radical regeneration in isoprene oxidation via peroxy radical isomerisations. II: Experimental evidence and global impact, *Phys. Chem. Chem. Phys.*, 12, 14227–14235, doi:10.1939/c0cp00811g, 2010.

Peeters, J., Vandenberg, S., Piessens, E., and Pultau, V.: H-atom abstraction in reactions of cyclic polyalkenes with OH, *Chemosphere*, 38, 1189–1195, 1999.

Peeters, J., Nguyen, T. L., and Vereecken, L.: HO_x radical regeneration in the oxidation of isoprene, *Phys. Chem. Chem. Phys.*, 11, 5935–5939, doi:10.1039/b908511d, 2009.

Peeters, J., Muller, J.-F., Stavrou, T., and Nguyen, V. S.: Hydroxyl radical recycling in isoprene oxidation driven by hydrogen bonding and hydrogen tunneling: the upgraded LIM1 mechanism, *J. Phys. Chem. A*, 118, 8625–8643, doi:10.1021/jp5033146, 2014.

Pollack, I., Lerner, B., and Ryerson, T.: Evaluation of ultraviolet light-emitting diodes for detection of atmospheric NO₂ by photolysis – chemiluminescence, *J. Atmos. Chem.*, 65, 111–125, doi:10.1007/s10874-011-9184-3, 2010.

Rivera-Rios, J. C., Nguyen, T. B., Crouse, J. D., Jud, W., St Clair, J. M., Mikoviny, T., Gilman, J. B., Lerner, B. M., Kaiser, J. B., de Gouw, J., Wisthaler, A., Hansel, A., Wennberg, P. O., Seinfeld, J. H., and Keutsch, F. N.: Conversion of hydroperoxides to carbonyls in field and laboratory instrumentation: observational bias in diagnosing pristine versus anthropogenically controlled atmospheric chemistry, *Geophys. Res. Lett.*, 41, 8645–8651, doi:10.1002/2014gl061919, 2014.

Roberts, J. M., Marchewka, M., Bertman, S. B., Goldan, P., Kuster, W., de Gouw, J., Warneke, C., Williams, E., Lerner, B., Murphy, P., Apel, E., and Fehsenfeld, F. C.: Analysis of the isoprene chemistry observed during the New England Air Quality Study (NEAQS) 2002 intensive experiment, *J. Geophys. Res.*, 111, D23S12, doi:10.1029/2006jd007570, 2006.

Ryerson, T., Huey, L., Knapp, K., Neuman, J., Parrish, D., Sueper, D., and Fehsenfeld, F.: Design and initial characterization of an inlet for gas-phase NO_y measurements from aircraft, *J. Geophys. Res.-Atmos.*, 104, 5483–5492, doi:10.1029/1998JD100087, 1999.

Shim, C., Wang, Y., Choi, Y., Palmer, P. I., Abbot, D. S., and Chance, K.: Constraining global isoprene emissions with Global Ozone Monitoring Experiment (GOME) formaldehyde column measurements, *J. Geophys. Res.*, 110, D24301, doi:10.1029/2004jd005629, 2005.

Stavrou, T., Müller, J.-F., De Smedt, I., Van Roozendaal, M., van der Werf, G. R., Giglio, L., and Guenther, A.: Evaluating the performance of pyrogenic and biogenic emission inventories against one decade of space-based formaldehyde columns, *Atmos. Chem. Phys.*, 9, 1037–1060, doi:10.5194/acp-9-1037-2009, 2009.

**Formaldehyde
production from
isoprene oxidation
across NO_x regimes**

G. M. Wolfe et al.

Title Page

Abstract

Introduction

Conclusions

References

Tables

Figures



Back

Close

Full Screen / Esc

Printer-friendly Version

Interactive Discussion



- Stavrakou, T., Müller, J.-F., Bauwens, M., De Smedt, I., Van Roozendael, M., Guenther, A., Wild, M., and Xia, X.: Isoprene emissions over Asia 1979–2012: impact of climate and land-use changes, *Atmos. Chem. Phys.*, 14, 4587–4605, doi:10.5194/acp-14-4587-2014, 2014.
- 5 Stroud, C., Roberts, J., Goldan, P., Kuster, W., Murphy, P., Williams, E., Hereid, D., Parrish, D., Sueper, D., Trainer, M., Fehsenfeld, F., Apel, E., Riemer, D., Wert, B., Henry, B., Fried, A., Martinez-Harder, M., Harder, H., Brune, W., Li, G., Xie, H., and Young, V.: Isoprene and its oxidation products, methacrolein and methylvinyl ketone, at an urban forested site during the 1999 Southern Oxidants Study, *J. Geophys. Res.-Atmos.*, 106, 8035–8046, doi:10.1029/2000JD900628, 2001.
- 10 Trainer, M., Williams, E., Parrish, D., Buhr, M., Allwine, E., Westberg, H., Fehsenfeld, F., and Liu, S.: Models and observations of the impact of natural hydrocarbons on rural ozone, *Nature*, 329, 705–707, doi:10.1038/329705a0, 1987.
- Wagner, N. L., Brock, C. A., Angevine, W. M., Beyersdorf, A., Campuzano-Jost, P., Day, D., de Gouw, J. A., Diskin, G. S., Gordon, T. D., Graus, M. G., Holloway, J. S., Huey, G., Jimenez, J. L., Lack, D. A., Liao, J., Liu, X., Markovic, M. Z., Middlebrook, A. M., Mikoviny, T., Peischl, J., Perring, A. E., Richardson, M. S., Ryerson, T. B., Schwarz, J. P., Warneke, C., Welti, A., Wisthaler, A., Ziemba, L. D., and Murphy, D. M.: In situ vertical profiles of aerosol extinction, mass, and composition over the southeast United States during SENEX and SEAC⁴RS: observations of a modest aerosol enhancement aloft, *Atmos. Chem. Phys.*, 15, 7085–7102, doi:10.5194/acp-15-7085-2015, 2015.
- 20 Warneke, C., de Gouw, J. A., Del Negro, L., Brioude, J., McKeen, S., Stark, H., Kuster, W. C., Goldan, P. D., Trainer, M., Fehsenfeld, F. C., Wiedinmyer, C., Guenther, A. B., Hansel, A., Wisthaler, A., Atlas, E., Holloway, J. S., Ryerson, T. B., Peischl, J., Huey, L. G., and Hanks, A. T. C.: Biogenic emission measurement and inventories determination of biogenic emissions in the eastern United States and Texas and comparison with biogenic emission inventories, *J. Geophys. Res.-Atmos.*, 115, D00F18, doi:10.1029/2009jd012445, 2010.
- 25 Warneke, C., Trainer, M., de Gouw, J. A., Parrish, D. D., Fahey, D., Ravishankara, A. R., Middlebrook, A. M., Brock, C. A., Roberts, J. M., Brown, S. S., Neuman, J. A., Lerner, B., Lack, D., Law, D., Hubler, G., Pollack, I., Sjostedt, S., Ryerson, T. B., Gilman, J. B., Liao, J., Holloway, J., Peischl, J., Nowak, J. B., Aikin, K., Min, K. E., Washenfelder, R. A., Graus, M., Richardson, M., Markovic, M., Wagner, N., Welti, A., Veres, P., Edwards, P., Schwarz, J. P., Gordon, T., Dube, W. B., McKeen, S., Brioude, J., Ahmadov, R., Bougiatioti, A., Lin, J., Nenes, A., Wolfe, G. M., Hanisco, T., Lee, B. H., Lopez-Hilfiker, F. D., Thornton, J., Keutsch, F., Kaiser, J.,

**Formaldehyde
production from
isoprene oxidation
across NO_x regimes**

G. M. Wolfe et al.

Title Page

Abstract

Introduction

Conclusions

References

Tables

Figures

◀

▶

◀

▶

Back

Close

Full Screen / Esc

Printer-friendly Version

Interactive Discussion



Mao, J., and Hatch, C. D.: Instrumentation and Measurement Strategy for the NOAA SENEX Aircraft Campaign as Part of the Southeast Atmosphere Study 2013, in preparation, 2015.

Wolfe, G. M., Crounse, J. D., Parrish, J. D., St. Clair, J. M., Beaver, M. R., Paulot, F., Yoon, T. P., Wennberg, P. O., and Keutsch, F. N.: Photolysis, OH reactivity and ozone reactivity of a proxy for isoprene-derived hydroperoxyenals (HPALDs), *Phys. Chem. Chem. Phys.*, 14, 7276–7286, doi:10.1039/c2cp40388a, 2012.

Wolfe, G. M., Cantrell, C., Kim, S., Mauldin III, R. L., Karl, T., Harley, P., Turnipseed, A., Zheng, W., Flocke, F., Apel, E. C., Hornbrook, R. S., Hall, S. R., Ullmann, K., Henry, S. B., DiGangi, J. P., Boyle, E. S., Kaser, L., Schnitzhofer, R., Hansel, A., Graus, M., Nakashima, Y., Kajii, Y., Guenther, A., and Keutsch, F. N.: Missing peroxy radical sources within a summer-time ponderosa pine forest, *Atmos. Chem. Phys.*, 14, 4715–4732, doi:10.5194/acp-14-4715-2014, 2014.

Xu, L., Guo, H., Boyd, C. M., Klein, M., Bougiatioti, A., Cerully, K. M., Hite, J. R., Isaacman-VanWertz, G., Kreisberg, N. M., Knote, C., Olson, K., Koss, A., Goldstein, A. H., Hering, S. V., de Gouw, J., Baumann, K., Lee, S.-H., Nenes, A., Weber, R. J., and Ng, N. L.: Effects of anthropogenic emissions on aerosol formation from isoprene and monoterpenes in the southeastern United States, *P. Natl. Acad. Sci. USA*, 112, 37–42, doi:10.1073/pnas.1417609112, 2015.

Formaldehyde production from isoprene oxidation across NO_x regimes

G. M. Wolfe et al.

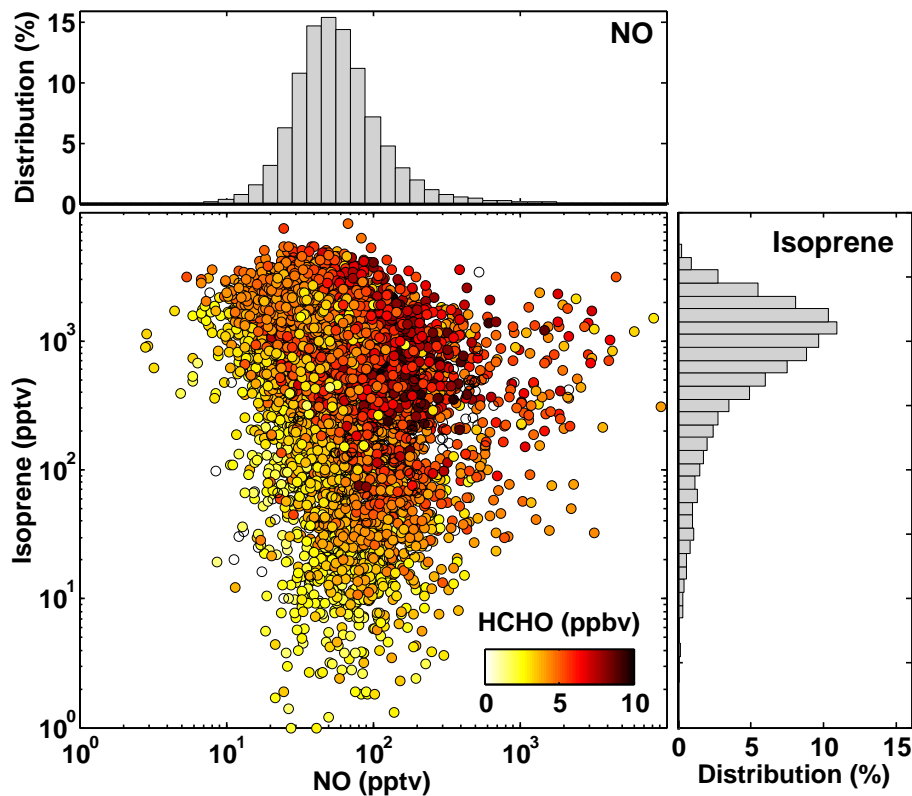
[Title Page](#)[Abstract](#)[Introduction](#)[Conclusions](#)[References](#)[Tables](#)[Figures](#)[◀](#)[▶](#)[◀](#)[▶](#)[Back](#)[Close](#)[Full Screen / Esc](#)[Printer-friendly Version](#)[Interactive Discussion](#)

Figure 1. Co-variation of isoprene, NO and HCHO mixing ratios in the summertime Southeast US Data are limited to daytime boundary layer observations. Histograms show the corresponding NO and isoprene distributions.

Formaldehyde production from isoprene oxidation across NO_x regimes

G. M. Wolfe et al.

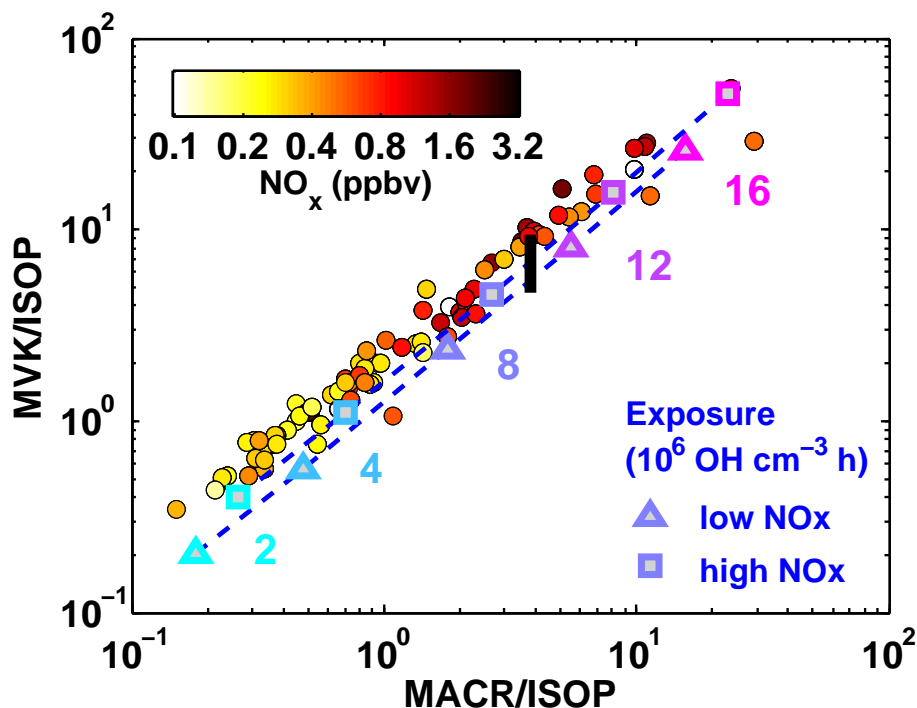


Figure 2. A photochemical clock of isoprene oxidation defined by the progression of daughter/parent ratios. Solid circles show the observed ratios calculated from iWAS observations, colored by NO_x . Blue/purple symbols, dashed lines, and text indicate the theoretical exposures (the product of OH concentration and time) corresponding to any given daughter/parent relationship. Theoretical values are calculated at 298 K using MVK and MACR yields for NO values of 50 pptv (triangles) and 1000 pptv (squares). The thick black line denotes the potential systematic error due to an upper-limit 51 % positive artifact in MVK observations (see Supplement).

Formaldehyde production from isoprene oxidation across NO_x regimes

G. M. Wolfe et al.

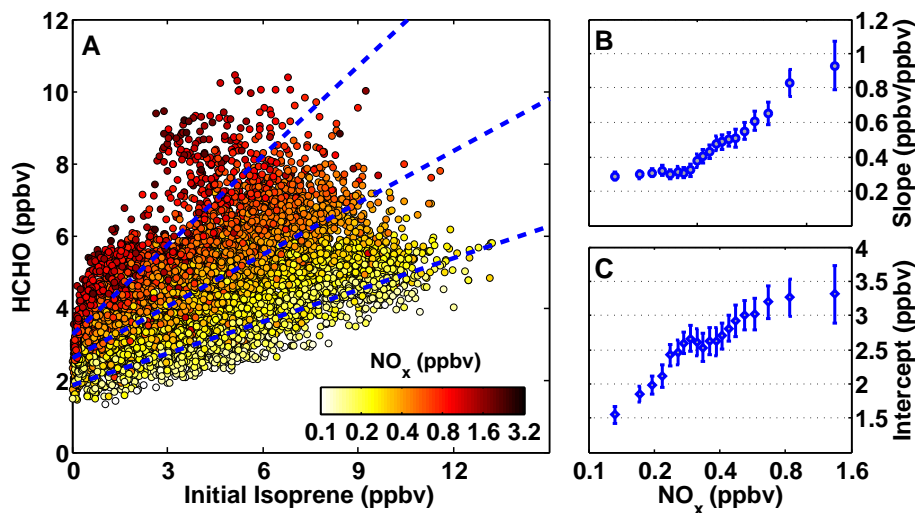


Figure 3. (a) NO_x modulates the relationship between observed HCHO and calculated initial isoprene mixing ratios. Symbols denote all 1 s data. Dashed lines illustrate representative major-axis fits of NO_x -grouped subsets at mean NO_x values of 170, 380 and 810 pptv (see text for details of fitting procedure). The slope (b) and intercept (c) of these fits are the prompt HCHO yield and background HCHO mixing ratio, respectively. Error bars in (b) and (c) are 3 σ fitting uncertainties.

[Title Page](#)[Abstract](#)[Introduction](#)[Conclusions](#)[References](#)[Tables](#)[Figures](#)[◀](#)[▶](#)[◀](#)[▶](#)[Back](#)[Close](#)[Full Screen / Esc](#)[Printer-friendly Version](#)[Interactive Discussion](#)

Formaldehyde production from isoprene oxidation across NO_x regimes

G. M. Wolfe et al.

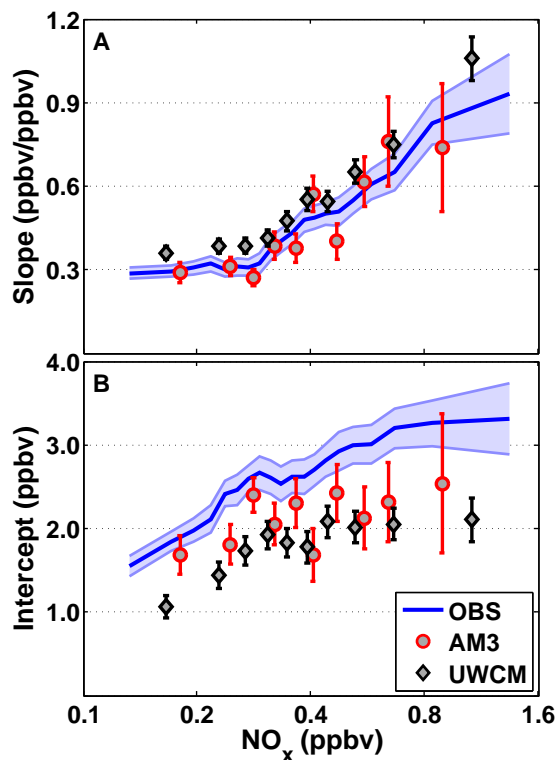


Figure 4. Comparison of observed and model-derived relationships between HCHO and initial isoprene vs. NO_x . Slopes (a) and intercepts (b) are calculated as described in the text. The observed values (blue line with shading) are the same as those shown in Fig. 3b and c. Symbols represent fit results for the global AM3 model (red circles) and the 0-D UWCM box model (black diamonds). Error bars denote 3σ fitting uncertainties.

Formaldehyde production from isoprene oxidation across NO_x regimes

G. M. Wolfe et al.

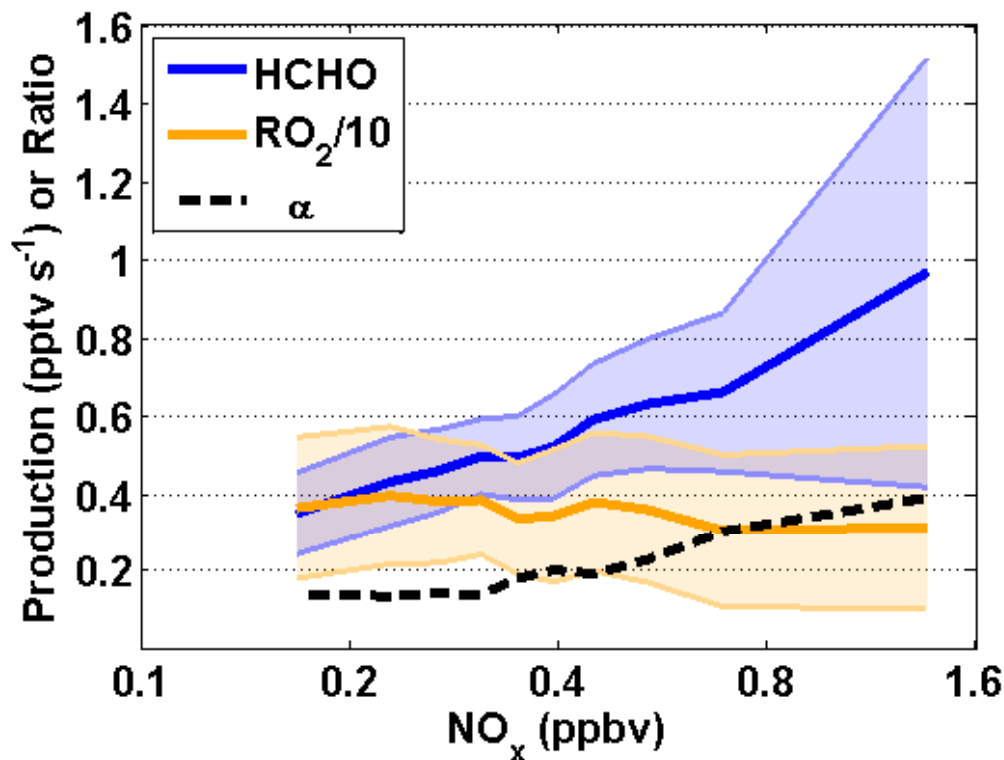


Figure 5. NO_x dependence of chemical properties related to HCHO production, extracted from the UWCM simulation of SENEX observations. Production rates for HCHO (blue) and total RO_2 (orange) are averaged over NO_x using 10 bins with equal numbers of points. Solid lines show the mean, shading is 1σ variability. Note that RO_2 production is scaled down by a factor of 10. The ratio of HCHO to RO_2 production gives the bulk HCHO branching ratio (dashed line).